PHYSICAL REVIEW B **91**, 205421 (2015)

Group theory for structural analysis and lattice vibrations in phosphorene systems

J. Ribeiro-Soares,[1,2,*] R. M. Almeida,[2] L. G. Cançado,[2] M. S. Dresselhaus,[3,4] and A. Jorio[2]

[1]*Departamento de Física, Universidade Federal de Lavras, Lavras, MG, 37200-000, Brazil*

[2]*Departamento de Física, Universidade Federal de Minas Gerais, Belo Horizonte, MG, 30123-970, Brazil*

[3]*Department of Electrical Engineering and Computer Science, Massachusetts Institute of Technology (MIT), Cambridge, Massachusetts 02139, USA*

[4]*Department of Physics, Massachusetts Institute of Technology (MIT), Cambridge, Massachusetts 02139, USA*

(Received 26 August 2014; revised manuscript received 10 April 2015; published 15 May 2015)

Group theory analysis for two-dimensional elemental systems related to phosphorene is presented, including (i) graphene, silicene, germanene, and stanene; (ii) their dependence on the number of layers; and (iii) their two possible stacking arrangements. Departing from the most symmetric D^1_{6h} graphene space group, the structures are found to have a group-subgroup relation, and analysis of the irreducible representations of their lattice vibrations makes it possible to distinguish between the different allotropes. The analysis can be used to study the effect of strain, to understand structural phase transitions, to characterize the number of layers, crystallographic orientation, and nonlinear phenomena.

DOI: 10.1103/PhysRevB.91.205421 PACS number(s): 61.46.−w, 63.22.Np, 68.35.Gy, 78.20.Ek

I. INTRODUCTION

Bulk phosphorus allotropes have been studied for 100 years [1,2], but it is only in the post-graphene era that their notable few-layer induced novel properties were placed under scrutiny. The two-dimensional ($2D$) monolayer counterpart of bulk black phosphorus [3], also called phosphorene (including the recently proposed "blue phosphorene" [4,5]), and the few-layer related systems have generated intense theoretical and experimental efforts addressing their optical [4–11], mechanical [9,12,13], thermal [13–15], and electrical [6,16–21] properties. Black phosphorus (black P) has shown highly anisotropic properties [4,7,12–15,18], in addition to a band gap that increases with a decreasing number of layers [from 0.3 eV (bulk) to 1.45eV for the monolayer [7,10,17]]. The role of strain in 2D structures is another relevant aspect and it has been shown to be valuable to tune optical properties [4,22–24].

Symmetry analysis has been used to understand the electronic structure of monolayer black P [11], and the Raman spectra of few-layer black P [25]. Blue phosphorene (blue P), which was found to be symmetrically compatible with the arsenic phase of phosphorus [3,26–28], is expected to exhibit a fundamental band gap that exceeds 2 eV [4,29]. A conversion route between the black and blue monolayer allotropes was already proposed, with stability and compatibility as in-plane heterostructures [4,29].

In this paper, group theory is used to obtain symmetry-related information for 2D black P, blue P, and related structures, including the dependence on the number of layers N and on the stacking arrangements. The related structures are the other 2D elemental structures, like graphene, silicene, germanene and stanene. Silicene and germanene have been recently synthesized [30–33], stanene is theoretically predicted [34], and all these structures exhibit the same lattice structure as a blue P monolayer. Therefore, the symmetry considerations for blue P discussed here are directly related to silicene, germanene, and stanene as well. Some considerations discussed here are adaptations from elemental aspects, which can be found in group theory books (Refs. [35–38]) and they can be used by students learning group theory, as well as by researchers working on layered compounds.

II. MONOLAYER GROUP-SUBGROUP RELATIONS

Black and blue P monolayers present real space lattices that resemble the graphene honeycomb lattice, but in a puckered structure. Schematics for the blue and black P are given in the top part of Fig. 1, and labeled accordingly. Light gray and black bullets indicate sets of atoms in different planes of the puckered structure. The red lines in the schematics show the top view of the unit cell. The black P monolayer primitive unit cell contains four atoms, while the blue P monolayer contains two atoms. The central schematics sketches the graphene structure, and dark gray bullets are used to indicate that all atoms are in the same plane.

Figure 1 shows a group-subgroup relation of the phosphorene parent materials, which are possible routes for structural modifications obtained via second-order phase transitions. Departing from the most symmetric D^1_{6h} graphene space group, which appears at the center of the 2D schematics in the top of Fig. 1, the left-side route is started by a uniaxial compression, while the right-side route is started by an isotropic lattice compression.

From the schematics on the top of Fig. 1, and departing from the D^1_{6h} central graphene structure to the left route, uniaxial compression induces a phase transition to subgroup D^{19}_{2h} of strained graphene. The hexagonal symmetry is lost, resulting in an orthorhombic structure where all atoms remain in the same plane. A possible and natural distortion of the orthorhombic lattice to accommodate uniaxial strain is the displacement of lines of atoms perpendicular to the strain direction, periodically up and down in the $\hat{z}$ direction (perpendicular to the 2D $\hat{x}\,\hat{y}$-plane structure), generating zigzag lines of atoms displaced

*Author to whom correspondence should be addressed: jenaina.soares@dfi.ufla.br

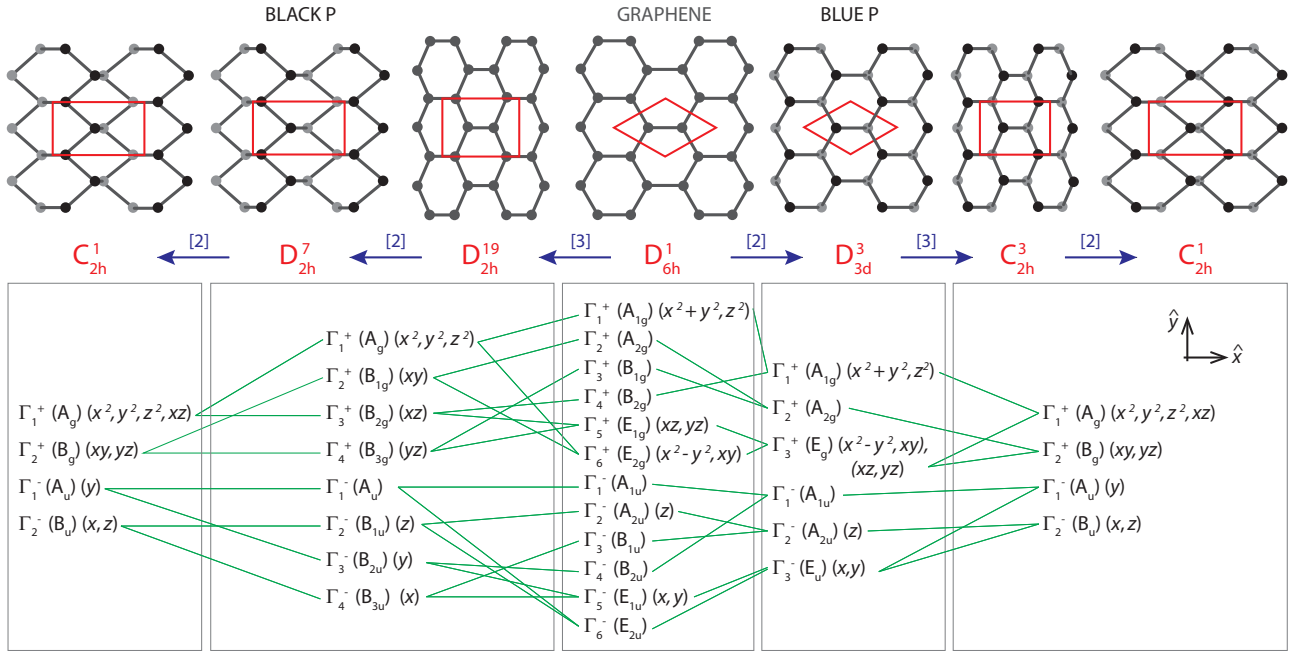

FIG. 1. (Color online) Group-subgroup correlation for phosphorene-related systems. From center to left: correlation between graphene (D^1_{6h} space group) and the black P monolayer (D^7_{2h}). The intermediate structure with the D^{19}_{2h} space group (and the same D_{2h} black P point group) occurs. A compressive strain in the $\hat{x}$ direction leads to a phase transition to the C^1_{2h} subgroup. From center to right: correlation between graphene (D^1_{6h} space group) and blue P monolayer (D^3_{3d}), followed by the blue P monolayer with a compressive strain in the $\hat{x}$ direction (C^3_{2h}). In a further loss of centering translations, the C^3_{2h} structure changes to the C^1_{2h} group. The top part brings structural schematics, while the bottom part displays the irreducible representations and the corresponding basis functions. The arrows indicate the sense of the lowering of symmetry, and the index of transformation of one group to another is indicated inside the brackets. To maintain the same axes orientations for the different structures, nonstandard settings are used [39]. The character tables are given in Appendix B.

to $+\hat{z}$ and $-\hat{z}$. Such a distortion generates the structure of black P, which belongs to the D^7_{2h} subgroup. A final distortion along this route can be obtained by a shear force, which displaces the top and bottom set of atoms in opposite directions, breaking the bonding symmetry of atoms aligned along the strain direction and separating the zigzag lines of atoms that are displaced up and down. The system then undergoes a phase transition to the C^1_{2h} subgroup.

Now on the right route shown in Fig. 1, departing again from the D^1_{6h} graphene structure, initially an isotropic strain changes the C-C bond distances, but it does not change the symmetry of the system (not shown in Fig. 1). However, a possible and natural distortion of the hexagonal lattice to accommodate such a strain is the displacement of atoms, periodically up and down in the $\pm\hat{z}$ directions, generating a trigonal arrangement of atoms. Such a distortion generates the structure of blue P (also of silicene, germanene and stanene), which belongs to the D^3_{3d} subgroup, with threefold rather than sixfold rotational symmetry. The number of atoms in the unit cell is unchanged. In sequence, if at that stage an uniaxial strain is applied, the system loses the threefold axis and undergoes a phase transition to the C^3_{2h} orthorhombic subgroup for the strained blue P. A final hypothetical distortion on the C^3_{2h} structure can lower the symmetry to a C^1_{2h} subgroup (last schematics on the right in Fig. 1).

The structure for the last schematics on the right in Fig. 1 belongs to the same space group as the strained and sheared black P (last schematics on the left in Fig. 1). Structural change between these two structures can be obtained via a first-order transition where the neighboring vertical lines of atoms exchange positions along z, possibly induced by a shear strain accompanied by compression perpendicular to the planes.

The bottom part of Fig. 1 shows the group-subgroup correlation between the irreducible representations (*IRs*) of the space groups. Some basis functions belonging to each *IR* are also displayed for all the groups. This information is a guide for the analysis of the phase transitions, for example, when using infrared (x,y,z basis) or Raman (quadratic basis) spectroscopies. Table I displays the irreducible representation

TABLE I. Irreducible representations for vibrational modes Γ^{vib} in the phosphorene-related space groups.

D^7_{2h}	$2\Gamma_1^+ \oplus \Gamma_2^+ \oplus 2\Gamma_3^+ \oplus \Gamma_4^+ \oplus \Gamma_1^- \oplus 2\Gamma_2^- \oplus \Gamma_3^- \oplus 2\Gamma_4^-$
D^{19}_{2h}	$\Gamma_1^+ \oplus \Gamma_2^+ \oplus \Gamma_2^- \oplus \Gamma_3^+ \oplus \Gamma_3^- \oplus \Gamma_4^-$
D^1_{6h}	$\Gamma_4^+ \oplus \Gamma_6^+ \oplus \Gamma_2^- \oplus \Gamma_5^-$
D^3_{3d}	$\Gamma_1^+ \oplus \Gamma_3^+ \oplus \Gamma_2^- \oplus \Gamma_3^-$
C^3_{2h}	$2\Gamma_1^+ \oplus \Gamma_2^+ \oplus \Gamma_1^- \oplus 2\Gamma_2^-$
C^1_{2h}	$4\Gamma_1^+ \oplus 2\Gamma_2^+ \oplus 2\Gamma_1^- \oplus 4\Gamma_2^-$

decomposition of the vibrational modes (Γ^{vib}). Excluding the acoustic modes, the remaining irreducible representations for a black P monolayer are $2\Gamma_1^+ \oplus \Gamma_2^+ \oplus 2\Gamma_3^+ \oplus \Gamma_4^+ \oplus \Gamma_1^- \oplus \Gamma_2^- \oplus \Gamma_4^-$, and for a blue P monolayer are $\Gamma_1^+ \oplus \Gamma_3^+$. While in the black P monolayer the one-dimensional representations $\Gamma_1^+, \Gamma_2^+, \Gamma_3^+$ and Γ_4^+ are Raman active, for the blue P monolayer only the Γ_1^+ and Γ_3^+ (where Γ_3^+ is doubly degenerate) modes are Raman active. The eigenvectors for black and blue P monolayer are illustrated in Appendix A.

The basis functions near each *IR* in the bottom part of Fig. 1 also guide the polarization dependent analysis in the back and forward Raman scattering configurations. We consider $\hat{z}$ as the light propagation direction, with $\hat{x}, \hat{y}$ as defined in Fig. 1. An xy polarization symbol indicates that the polarization of the incident light is in the x direction, and the polarization of the scattered light, in the y direction. For the blue P monolayer, the Γ_1^+ mode is detectable under xx and yy polarizations, and the Γ_3^+ mode is detectable under xx, yy, and xy polarizations. In the black P monolayer, the Γ_1^+ modes are detectable under xx and yy geometries, while the Γ_2^+ mode is detectable in the xy configuration. Therefore polarization can be used to distinguish black and blue P monolayers from one another. Infrared spectroscopy is also different for the two allotropes: the black P monolayer shows $\Gamma_2^- \oplus \Gamma_4^-$ modes that are infrared active, while the blue P does not show any infrared-active mode. In addition, the dependence with polarization can be used to identify the crystallographic orientation of each one of these allotropes.

The *IR* group-subgroup correlations are given by the lines connecting *IRs* in Fig. 1. For example, the application of an uniaxial strain to a blue P monolayer, with the D_{3d}^3 space group, generates a new structure with a C_{2h}^3 space group symmetry. The optical modes for the C_{2h}^3 structure are given by $2\Gamma_1^+ \oplus \Gamma_2^+$, in contrast with the previous $\Gamma_1^+ \oplus \Gamma_3^+$ of the unstrained structure. The maximum intensity in polarized Raman experiments occurs under the xy configuration for the Γ_2^+ mode, and under the xx, yy, and xy configurations for the Γ_3^+ mode. Furthermore, the lowering of symmetry in the strained structure lifts the degeneracy of the Γ_3^+ mode, thereby giving rise to two one-dimensional irreducible representations. The strain-induced symmetry breaking and the consequent breaking of the vibration mode degeneracies are reported in other 2D structures, like transition metal dichalcogenides [24] and graphene [43,44]. For these materials, polarized Raman spectroscopy is recognized as a purely optical method for the determination of the crystallographic orientation and strain level. For blue P monolayer, depending on the peak frequency difference of the two new one-dimensional irreducible representations and their intensities, it is expected to be possible to realize a similar structural and strain analysis.

III. MULTIPLE LAYERS AND DIFFERENT STACKING ORDERS OF BLACK AND BLUE PHOSPHORENE

For a more complete characterization of black and blue phosphorus systems, it is important to extend the above symmetry analysis to multiple layers, considering different stacking orders, as shown in Fig 2. The space groups and the irreducible representations of the vibrational modes of these N-layer systems are given in Table II.

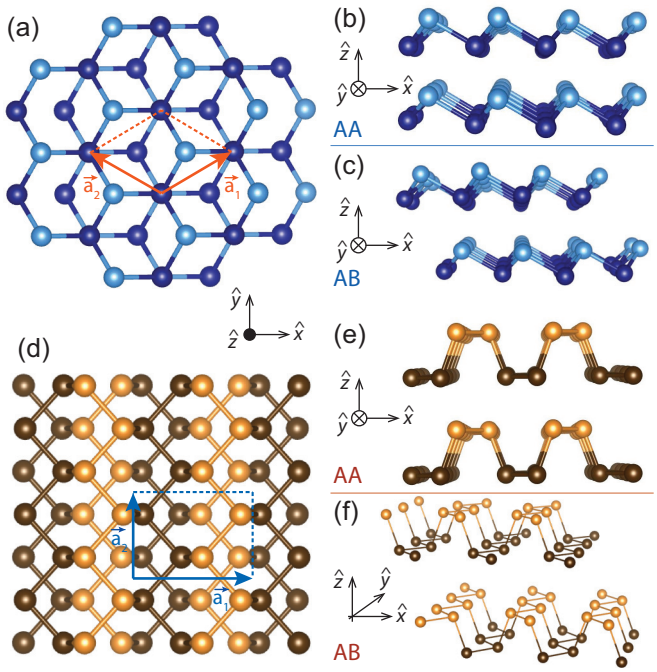

FIG. 2. (Color online) Lattice structure of bilayer phosphorene. Color and shading are used to indicate the top and bottom atoms of the nonplanar layers. (a) Top view of the AB stacking for blue phosphorus bilayer. (b) and (c) Side view of the AA and AB stacking, respectively, for blue phosphorous. (d) Top view of the AB stacking for black phosphorus bilayer. (e) and (f) Side view of the AA and AB stacking arrangements, respectively, for black phosphorous bilayer.

Figures 2(a,c) and 2(b) show, respectively, the AB and AA stacking arrangements of black P, while Figs. 2(d,f) and 2(e) illustrate the corresponding stacks for blue P. The AA stacking for both allotropes occurs when two monolayer units are piled up, with each atom of the first monolayer on top of a corresponding atom in the second layer. The top view of the AA stacking arrangement, for both black and blue P, is identical to the monolayer seen in Fig. 1. In the AB stacking of black P, the second (top) layer is displaced from the first (bottom) layer by half of the primitive lattice vector $\vec{a}_2$, as shown in Fig. 2(d). In blue P, an atom of the top layer is placed on top of a noncorresponding atom in the bottom layer, in the other sublattice [see Fig. 2(a)].

The results presented in Table II show that different numbers of layers and different stacking arrangements can also result in symmetry variations, and the differences depend on whether N is even or odd. For the AA stacking, an odd and even number N of layers have the same space group (D_{3d}^3 and D_{2h}^7 for blue and black P, respectively). The number of modes for N odd and even increases with increasing N, following the difference in the number of atoms/unit cell.

In AB black P, the N-layered structures can be obtained from exfoliation of the bulk $A17$ phase [D_{2h}^{18} ($Aema$, #64)], and the space groups for N odd and N even layers are subgroups of the bulk space group. For AB bulk black P, $\Gamma^{vib} = 2\Gamma_1^+ \oplus \Gamma_2^+ \oplus 2\Gamma_3^+ \oplus \Gamma_4^+ \oplus \Gamma_1^- \oplus 2\Gamma_2^- \oplus \Gamma_3^- \oplus 2\Gamma_4^-$ (for Γ^{vib} in the standard setting, see Ref. [45]). Only the $\Gamma_1^+(A_g)$ (xx and yy polarizations) and $\Gamma_2^+(B_{1g})$ (xy polarization) modes are Raman

TABLE II. Space groups and irreducible representations for vibrational modes (Γ^{vib}), according to the allotrope (black P, blue P, silicene, germanene and stanene), to the number N of layers and to the stacking order.

Black P		
	AA	AB
N odd	$[D_{2h}^{7}\ (Pbmn, \#53)]$[a] $2N(\Gamma_1^+ \oplus \Gamma_3^+ \oplus \Gamma_2^- \oplus \Gamma_4^-)$ $\oplus N(\Gamma_2^+ \oplus \Gamma_4^+ \oplus \Gamma_1^- \oplus \Gamma_3^-)$[b]	$[D_{2h}^{7}\ (Pbmn, \#53)]$ $2N(\Gamma_1^+ \oplus \Gamma_3^+ \oplus \Gamma_2^- \oplus \Gamma_4^-)$ $\oplus N(\Gamma_2^+ \oplus \Gamma_4^+ \oplus \Gamma_1^- \oplus \Gamma_3^-)$
N even		$[D_{2h}^{11}\ (Pbma, \#57)]$ $2N(\Gamma_1^+ \oplus \Gamma_3^+ \oplus \Gamma_2^- \oplus \Gamma_4^-)$ $\oplus N(\Gamma_2^+ \oplus \Gamma_4^+ \oplus \Gamma_1^- \oplus \Gamma_3^-)$
Blue P, silicene, germanene and stanene		
	AA	AB
$N = 1$	$[D_{3d}^{3}\ (P\bar{3}m1, \#164)]$ $N(\Gamma_1^+ \oplus \Gamma_3^+ \oplus \Gamma_2^- \oplus \Gamma_3^-)$	$[D_{3d}^{3}\ (P\bar{3}m1, \#164)]$ $\Gamma_1^+ \oplus \Gamma_3^+ \oplus \Gamma_2^- \oplus \Gamma_3^-$
N odd ($\neq 1$)		$[C_{3v}^{1}\ (P3m1, \#156)]$ $2N(\Gamma_1 \oplus \Gamma_3)$
N even		$[D_{3d}^{3}\ (P\bar{3}m1, \#164)]$ $N(\Gamma_1^+ \oplus \Gamma_3^+ \oplus \Gamma_2^- \oplus \Gamma_3^-)$

[a]Notation: Schoenflies symbol, Hermann-Mauguin symbol, International Tables for Crystallography space group #, Vol. A (ITCA) [39] - Vol. E (ITCE) [40] for "layered subperiodic groups" could be used, but ITCA leads to an immediate comparison with the literature [41,42]. One-to-one correlation exists when limited to the Brilluoin zone center.

[b]Space group (SG) notation. Conversion to point group (PG) notation, and convenient basis functions for each irreducible representation are given in Appendix B.

active (in the back and forward Raman scattering geometries), and for both N odd and even, these modes correspond to Γ_1^+ and Γ_2^+, respectively.

On the other hand, for blue P, the AB stacking arrangement shows different space groups depending on the number of layers. The AB stacking of blue P is related to the $A7$ phosphorus phase [D_{3d}^{5} ($R\bar{3}m$, #166) space group, which can be treated as the ABC stacking of 3 blue P monolayer units]. It is possible to establish a correlation between the bulk ABC stacking and the bilayer AB stacking (see Appendix B). The Γ^{vib} for these two systems differs only in the total number of modes due to the change in the number of atoms in the primitive unit cell. Information from Table II shows a different number of predicted modes and symmetry variations depending on the number of layers for both the AA and AB stacking arrangements of black and blue P with few-layers, and a layer-number dependent comparison analysis can be performed. For AA and AB blue P stacking, as well as for AA black P stacking, to the best of our knowledge, a bulk counterpart has not yet been synthesized.

IV. INVERSION SYMMETRY

The presence or absence of inversion is another symmetry-dependent property that can vary with the allotrope, the stacking order, and layer number N. In Table II, the inversion symmetry is absent only for the N odd ($N > 1$) AB stacked blue P C_{3v}^{1} structure. The absence of inversion symmetry in the monolayer version of some transition metal dichalcogenides (TMDs) [42] made it possible to couple spin and valley physics, opening new perspectives for spintronic and valleytronic devices [46,47]. Furthermore, the absence of inversion symmetry in N odd layers of TMDs has been used in the study of nonlinear optical properties by means of second harmonic generation (SHG) [48–50]. In Table II, the structure in which the inversion symmetry is absent is expected to show a significant SHG signal, while the centrosymmetric crystals must show no signal. It is interesting to note that the absence of inversion occurs for N odd layers in the AB blue P (excluding $N = 1$). The analysis of the presence versus absence of the inversion operation for N odd and even layers in the same stacking arrangement based on SHG measurements can, therefore, be used to characterize the crystallographic orientation and number of layers for the AB stacking of blue P.

V. CONCLUSION

In summary, we have used group theory to gain insights into the symmetry aspects of black P, blue P, graphene, silicene, germanene, and stanene, and their few-layer related systems, in two different stacking arrangements. Our analysis can be used to distinguish the different systems, and for a fast characterization of in-plane heterostructures that can be built to customize certain desired properties in these new few layered materials. Strained black P and blue P monolayers may exhibit the C_{2h}^{1} subgroup in common. Previous theoretical results suggested a possible conversion trajectory process from black to blue P monolayer [4], which corresponds to specific changes in the atomic positions and the stretching of the black P monolayer to obtain blue phosphorene. The group-subgroup relations shown here corroborate the hypothesis of a mechanical conversion route [4]. The analysis of inversion symmetry-breaking offers another possibility for identifying the number of layers and their crystallographic orientation, in addition to exploring nonlinear optical phenomena.

ACKNOWLEDGMENTS

We would like to strongly acknowledge P. Li, I. Appelbaum and A-L. Phaneuf-L'Heureux for a critical reading of the manuscript, and N. L. Speziali for discussions. The authors acknowledge financial support from FAPEMIG, CNPq Grant 551953/2011-0, and NSF (USA), DMR-1004147.

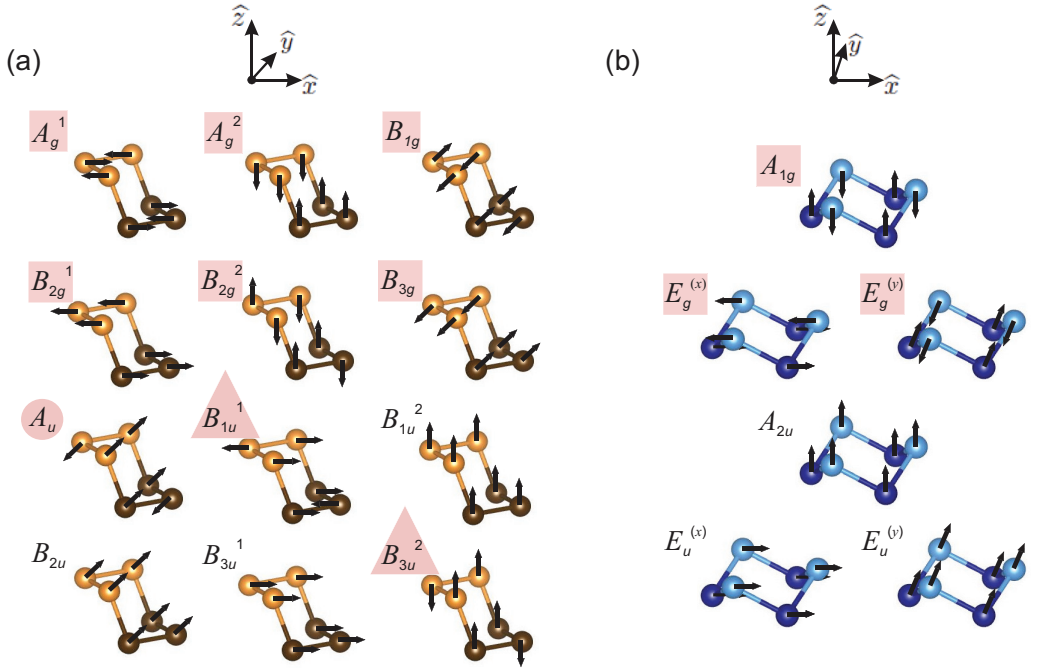

FIG. 3. (Color online) Non-normalized eigenvector representations for black (a) and blue (b) P monolayer vibrational modes, in their respective axis choices. Pink rectangles indicate Raman active modes, pink triangles represent infrared active modes and pink circles indicate silent modes. The remaining modes are acoustic modes.

APPENDIX A: MONOLAYER BLACK P AND BLUE P EIGENVECTORS

Figures 3(a) and 3(b) shows the phonon eigenvectors for black and blue phosphorous, respectively.

APPENDIX B: CHARACTER TABLES WITH SPACE GROUP (SG) TO POINT GROUP (PG) NOTATION CONVERSION WITH CONVENIENT BASIS FUNCTIONS AND MODE ACTIVITY CLASSIFICATION LIST

The tables shown here were prepared by adapting the point group tables presented in group theory books [35–38] to the case of the specific space groups used in this work. Mode activity tables are given for as well.

(1) Character table and mode activity for D_{6h}^1 and D_{2h}^{19} space groups

(a) D_{6h}^1 (Tables III and IV):

(b) D_{2h}^{19} (Tables V and VI):

(2) Blue phosphorus monolayer under strain [C_{2h}^1 (Tables VII and IX) and C_{2h}^3 (Table VIII) space groups]

The character table for the C_{2h}^1 group is used in connection with the C_{2h}^3 ($C2/m$, #12) space group, in which additional symmetry operations associated with a centering translation [centering vector: $(\frac{1}{2},\frac{1}{2},0)$] occurs, but the point group is the same for both C_{2h}^1 and C_{2h}^3.

(3) Black phosphorus for N odd and N even number of layers (D_{2h}^7 and D_{2h}^{11} space groups)

(a) AA stacking for N even and N odd, and AB stacking for N odd (Tables X and XI);

(b) AB stacking for N even (Tables XII and XIII);

(4) Blue phosphorus, silicene, germanene, and stanene for N odd and N even number of layers (D_{3d}^3 and C_{3v}^1 space groups, respectively)

(a) AA stacking for N even and N odd, and AB stacking for monolayer and N even (Tables XIV and XV);

(b) AB stacking for N odd (Tables XVI and XVII);

(5) Bulk counterparts

(a) $A17$ phase [black phosphorus, D_{2h}^{18} ($Aema$, #64) Tables XVIII and XIX];

(b) $A7$ phase [ABC stacking, D_{3d}^5 ($R\bar{3}m$, #166) and its relation with the AB blue phosphorus bilayer, Table XX.]

The point group for the $A7$ phase of phosphorus is D_{3d}, and the character table possesses the same characters as the table for AA blue phosphorus stacking [D_{3d}^3 ($P\bar{3}m1$, #164)]. Due to this fact, the irreducible representations are the same and the Γ^{vib} differs only in the number of modes. The classification of the modes is given in Table XX.

TABLE III. Character table for the Γ point [D^1_{6h} ($P6/mmm$, #191)].

SG	PG	E	C_3^+ C_3^-	C_2	C_6^- C_6^+	$C_2'^A$ $C_2'^B$ $C_2'^C$	$C_2''^A$ $C_2''^B$ $C_2''^C$	i	S_6^+ S_6^-	σ_h	S_3^- S_3^+	σ_d^A σ_d^B σ_d^C	σ_v^A σ_v^B σ_v^C	Basis
Γ_1^+	A_{1g}	1	1	1	1	1	1	1	1	1	1	1	1	x^2+y^2, z^2
Γ_2^+	A_{2g}	1	1	1	1	−1	−1	1	1	1	1	−1	−1	
Γ_3^+	B_{1g}	1	1	−1	−1	−1	1	1	1	−1	−1	−1	1	
Γ_4^+	B_{2g}	1	1	−1	−1	1	−1	1	1	−1	−1	1	−1	
Γ_5^+	E_{1g}	2	−1	−2	1	0	0	2	−1	−2	1	0	0	(xz,yz)
Γ_6^+	E_{2g}	2	−1	2	−1	0	0	2	−1	2	−1	0	0	(x^2-y^2,xy)
Γ_1^-	A_{1u}	1	1	1	1	1	1	−1	−1	−1	−1	−1	−1	
Γ_2^-	A_{2u}	1	1	1	1	−1	−1	−1	−1	−1	−1	1	1	z
Γ_3^-	B_{1u}	1	1	−1	−1	−1	1	−1	−1	1	1	1	−1	
Γ_4^-	B_{2u}	1	1	−1	−1	1	−1	−1	−1	1	1	−1	1	
Γ_5^-	E_{1u}	2	−1	−2	1	0	0	−2	1	2	−1	0	0	(x,y)
Γ_6^-	E_{2u}	2	−1	2	−1	0	0	−2	1	−2	1	0	0	

TABLE IV. Normal vibrational mode irreducible representations (Γ^{vib}) for graphene. Irreducible representations for the Raman active, infrared active, acoustic, and silent modes are identified.

D^1_{6h} ($P6/mmm$, #191)	
Γ^{vib}	$\Gamma_4^+ \oplus \Gamma_6^+ \oplus \Gamma_2^- \oplus \Gamma_5^-$
Raman	Γ_6^+
Infrared	–
Acoustic	$\Gamma_2^- \oplus \Gamma_5^-$
Silent	Γ_4^+

TABLE V. Character table for the Γ point [D^{19}_{2h} ($Cmmm$, #65)]. The symmetry operations associated with the centering translation [centering vector: ($\frac{1}{2}$, $\frac{1}{2}$,0)] are not shown.

SG	PG	$\{E\|0\}$	$\{C_{2\hat{z}}\|0\}$	$\{C_{2\hat{y}}\|0\}$	$\{C_{2\hat{x}}\|0\}$	$\{i\|0\}$	$\{\sigma_{xy}\|0\}$	$\{\sigma_{xz}\|0\}$	$\{\sigma_{yz}\|0\}$	Basis
Γ_1^+	A_g	1	1	1	1	1	1	1	1	x^2,y^2,z^2
Γ_2^+	B_{1g}	1	1	−1	−1	1	1	−1	−1	xy
Γ_3^+	B_{2g}	1	−1	1	−1	1	−1	1	−1	xz
Γ_4^+	B_{3g}	1	−1	−1	1	1	−1	−1	1	yz
Γ_1^-	A_u	1	1	1	1	−1	−1	−1	−1	
Γ_2^-	B_{1u}	1	1	−1	−1	−1	−1	1	1	z
Γ_3^-	B_{2u}	1	−1	1	−1	−1	1	−1	1	y
Γ_4^-	B_{3u}	1	−1	−1	1	−1	1	1	−1	x

TABLE VI. Normal vibrational mode irreducible representations (Γ^{vib}) for strained graphene. Irreducible representations for the Raman active, infrared active, acoustic, and silent modes are identified.

D^{19}_{2h} ($Cmmm$, #65)	
Γ^{vib}	$\Gamma_1^+ \oplus \Gamma_2^+ \oplus \Gamma_3^+ \oplus \Gamma_2^- \oplus \Gamma_3^- \oplus \Gamma_4^-$
Raman	$\Gamma_1^+ \oplus \Gamma_2^+ \oplus \Gamma_3^+$
Infrared	–
Acoustic	$\Gamma_2^- \oplus \Gamma_3^- \oplus \Gamma_4^-$
Silent	–

TABLE VII. Character table for the Γpoint [C_{2h}^1(P2/m,#10)].

SG	PG	$\{E\|0\}$	$\{C_{2\hat{y}}\|0\}$	$\{\sigma_{xz}\|0\}$	$\{i\|0\}$	Basis
Γ_1^+	A_g	1	1	1	1	x^2,y^2,z^2,xz
Γ_1^-	A_u	1	1	−1	−1	y
Γ_2^+	B_g	1	−1	−1	1	xy,yz
Γ_2^-	B_u	1	−1	1	−1	x,z

TABLE VIII. Normal vibrational mode irreducible representations (Γ^{vib}) for strained (or stressed) blue P monolayer at the Γ point (C_{2h}^3). Irreducible representations for the Raman active, infrared active, acoustic, and silent modes are identified.

C_{2h}^3 ($C2/m$, #12)	
Γ^{vib}	$2\Gamma_1^+ \oplus 2\Gamma_2^- \oplus \Gamma_1^- \oplus \Gamma_2^+$
Raman	$2\Gamma_1^+ \oplus \Gamma_2^+$
Infrared	–
Acoustic	$\Gamma_1^- \oplus 2\Gamma_2^-$
Silent	–

TABLE IX. Normal vibrational mode irreducible representations (Γ^{vib}) for strained (or stressed) and distorted blue P monolayer at the Γ point (C_{2h}^1). Irreducible representations for the Raman active, infrared active, acoustic, and silent modes are identified.

C_{2h}^1 ($P2/m$, #10)	
Γ^{vib}	$4\Gamma_1^+ \oplus 4\Gamma_2^- \oplus 2\Gamma_1^- \oplus 2\Gamma_2^+$
Raman	$4\Gamma_1^+ \oplus 2\Gamma_2^+$
Infrared	$2\Gamma_2^- \oplus 1\Gamma_1^-$
Acoustic	$2\Gamma_2^- \oplus 1\Gamma_1^-$
Silent	–

TABLE X. Character table for the Γ point [D_{2h}^7 ($Pbmn$, #53)].

SG	PG	$\{E\|0\}$	$\{C_{2\hat{z}(x=y=1/4)}\|0\}$	$\{C_{2\hat{y}}\|0\}$	$\{C_{2\hat{x}(y=\frac{1}{4})}\|\tau_x\}$[a]	$\{i\|0\}$	$\{\sigma_{xy}\|\tau_n\}$[b]	$\{\sigma_{xz}\|0\}$	$\{\sigma_{yz(x=\frac{1}{4})}\|\tau_y\}$[c]	Basis
Γ_1^+	A_g	1	1	1	1	1	1	1	1	x^2,y^2,z^2
Γ_2^+	B_{1g}	1	1	−1	−1	1	1	−1	−1	xy
Γ_3^+	B_{2g}	1	−1	1	−1	1	−1	1	−1	xz
Γ_4^+	B_{3g}	1	−1	−1	1	1	−1	−1	1	yz
Γ_1^-	A_u	1	1	1	1	−1	−1	−1	−1	
Γ_2^-	B_{1u}	1	1	−1	−1	−1	−1	1	1	z
Γ_3^-	B_{2u}	1	−1	1	−1	−1	1	−1	1	y
Γ_4^-	B_{3u}	1	−1	−1	1	−1	1	1	−1	x

[a] τ_x is the translation of half of the a_1 lattice parameter along the $\hat{x}$ direction [$\tau_x = (\frac{1}{2})a_1\hat{x}$].
[b] τ_n is the translation of half of the a_1 lattice parameter along the $\hat{x}$ direction and the translation of half of the a_2 lattice parameter along the $\hat{y}$ direction [$\tau_n = (\frac{1}{2})a_1\hat{x} + (\frac{1}{2})a_2\hat{y}$].
[c] τ_y is the translation of half of the a_2 lattice parameter along the $\hat{y}$ direction [$\tau_y = (\frac{1}{2})a_2\hat{y}$].

TABLE XI. Normal vibrational mode irreducible representations (Γ^{vib}) for black phosphorus AA stacking (N even and N odd), and AB stacking (N odd) at the Γ point. Irreducible representations for the Raman active, infrared active, acoustic and silent modes are identified.

D_{2h}^{7} ($Pbmn$, #53)		
	Γ^{vib}	$2N(\Gamma_1^+ \oplus \Gamma_3^+ \oplus \Gamma_2^- \oplus \Gamma_4^-) \oplus N(\Gamma_2^+ \oplus \Gamma_4^+ \oplus \Gamma_1^- \oplus \Gamma_3^-)$
	Raman	$2N(\Gamma_1^+ \oplus \Gamma_3^+) \oplus N(\Gamma_2^+ \oplus \Gamma_4^+)$
	Infrared	$(2N-1)(\Gamma_2^- \oplus \Gamma_4^-) \oplus (N-1)\Gamma_3^-$
	Acoustic	$\Gamma_2^- \oplus \Gamma_3^- \oplus \Gamma_4^-$
	Silent	$N\Gamma_1^-$

TABLE XII. Character table for the Γ point [D_{2h}^{11} ($Pbma$, #57)].

SG	PG	$\{E\|0\}$	$\{C_{2\hat{z}(x=\frac{1}{4})}\|0\}$	$\{C_{2\hat{y}}\|\tau_y\}$[a]	$\{C_{2\hat{x}(y=\frac{1}{4})}\|\tau_x\}$[b]	$\{i\|0\}$	$\{\sigma_{xy}\|\tau_x\}$[b]	$\{\sigma_{xz(y=\frac{1}{4})}\|0\}$	$\{\sigma_{yz(x=\frac{1}{4})}\|\tau_y\}$[a]	Basis
Γ_1^+	A_g	1	1	1	1	1	1	1	1	x^2, y^2, z^2
Γ_2^+	B_{1g}	1	1	−1	−1	1	1	−1	−1	xy
Γ_3^+	B_{2g}	1	−1	1	−1	1	−1	1	−1	xz
Γ_4^+	B_{3g}	1	−1	−1	1	1	−1	−1	1	yz
Γ_1^-	A_u	1	1	1	1	−1	−1	−1	−1	
Γ_2^-	B_{1u}	1	1	−1	−1	−1	−1	1	1	z
Γ_3^-	B_{2u}	1	−1	1	−1	−1	1	−1	1	y
Γ_4^-	B_{3u}	1	−1	−1	1	−1	1	1	−1	x

[a] τ_y is the translation of half of the a_2 lattice parameter along the $\hat{y}$ direction [$\tau_y = (\frac{1}{2})a_2\hat{y}$].
[b] τ_x is the translation of half of the a_1 lattice parameter along the $\hat{x}$ direction [$\tau_x = (\frac{1}{2})a_1\hat{x}$].

TABLE XIII. Normal vibrational mode irreducible representations (Γ^{vib}) for black phosphorus AB stacking (N even) at the Γ point. Irreducible representations for the Raman active, infrared active, acoustic, and silent modes are identified.

D_{2h}^{11} ($Pbma$, #57)		
	Γ^{vib}	$2N(\Gamma_1^+ \oplus \Gamma_3^+ \oplus \Gamma_2^- \oplus \Gamma_4^-) \oplus N(\Gamma_2^+ \oplus \Gamma_4^+ \oplus \Gamma_1^- \oplus \Gamma_3^-)$
	Raman	$2N(\Gamma_1^+ \oplus \Gamma_3^+) \oplus N(\Gamma_2^+ \oplus \Gamma_4^+)$
	Infrared	$(2N-1)(\Gamma_2^- \oplus \Gamma_4^-) \oplus (N-1)\Gamma_3^-$
	Acoustic	$\Gamma_2^- \oplus \Gamma_3^- \oplus \Gamma_4^-$
	Silent	$N\Gamma_1^-$

TABLE XIV. Character table for the Γ point [D_{3d}^{3} ($P\bar{3}m1$, #164)].

SG	PG	E	C_3^+ C_3^-	$C_2'^A$ $C_2'^B$ $C_2'^C$	i	S_6^+ S_6^-	σ_d^A σ_d^B σ_d^C	Basis
Γ_1^+	A_{1g}	1	1	1	1	1	1	x^2+y^2, z^2
Γ_2^+	A_{2g}	1	1	−1	1	1	−1	
Γ_3^+	E_g	2	−1	0	2	−1	0	$(xz, yz), (x^2-y^2, xy)$
Γ_1^-	A_{1u}	1	1	1	−1	−1	−1	
Γ_2^-	A_{2u}	1	1	−1	−1	−1	1	z
Γ_3^-	E_u	2	−1	0	−2	1	0	(x, y)

TABLE XV. Normal vibrational mode irreducible representations (Γ^{vib}) for blue phosphorus, silicene, germanene, and stanene AA stacking (N even and N odd), and AB stacking (monolayer and N even) at the Γ point. Irreducible representations for the Raman active, infrared active, acoustic, and silent modes are identified.

D_{3d}^3 ($P\bar{3}m1$, #164)	
Γ^{vib}	$N(\Gamma_1^+ \oplus \Gamma_3^+ \oplus \Gamma_2^- \oplus \Gamma_3^-)$
Raman	$N(\Gamma_1^+ \oplus \Gamma_3^+)$
Infrared	$(N-1)(\Gamma_2^- \oplus \Gamma_3^-)$
Acoustic	$\Gamma_2^- \oplus \Gamma_3^-$
Silent	–

TABLE XVI. Character table for the Γ point [C_{3v}^1 ($P3m1$, #156)].

SG	PG	E	C_3^+ C_3^-	σ_d^A σ_d^B σ_d^C	Basis
Γ_1	A_1	1	1	1	z,x^2+y^2,z^2
Γ_2	A_2	1	1	−1	
Γ_3	E	2	−1	0	(xz,yz),(x,y) (x^2-y^2,xy)

TABLE XVII. Normal vibrational mode irreducible representations (Γ^{vib}) for blue phosphorus, silicene, germanene, and stanene AB stacking (N odd) at the Γ point. Irreducible representations for the Raman active, infrared active, acoustic and silent modes are identified.

C_{3v}^1 ($P3m1$, #156)	
Γ^{vib}	$2N(\Gamma_1 \oplus \Gamma_3)$
Raman	$(2N-1)(\Gamma_1 \oplus \Gamma_3)$
Infrared	$(2N-1)(\Gamma_1 \oplus \Gamma_3)$
Acoustic	$\Gamma_1 \oplus \Gamma_3$
Silent	–

TABLE XVIII. Character table for the Γ point [D_{2h}^{18} ($Aema$, #64)]. The symmetry operations associated with the centering translation [centering vector: $(0,\frac{1}{2},\frac{1}{2})$] are not shown.

SG	PG	$\{E\|0\}$	$\{C_{2\hat{z}(x=\frac{1}{4})}\|\tau_z\}$[a]	$\{C_{2\hat{y}}\|0\}$	$\{C_{2\hat{x}(z=\frac{1}{4})}\|\tau_x\}$[b]	$\{i\|0\}$	$\{\sigma_{xy(z=1/4)}\|\tau_x\}$[b]	$\{\sigma_{xz}\|0\}$	$\{\sigma_{yz(x=\frac{1}{4})}\|\tau_z\}$[a]	Basis
Γ_1^+	A_g	1	1	1	1	1	1	1	1	x^2,y^2,z^2
Γ_2^+	B_{1g}	1	1	−1	−1	1	1	−1	−1	xy
Γ_3^+	B_{2g}	1	−1	1	−1	1	−1	1	−1	xz
Γ_4^+	B_{3g}	1	−1	−1	1	1	−1	−1	1	yz
Γ_1^-	A_u	1	1	1	1	−1	−1	−1	−1	
Γ_2^-	B_{1u}	1	1	−1	−1	−1	−1	1	1	z
Γ_3^-	B_{2u}	1	−1	1	−1	−1	1	−1	1	y
Γ_4^-	B_{3u}	1	−1	−1	1	−1	1	1	−1	x

[a] τ_z is the translation of half of the c lattice parameter along the $\hat{z}$ direction [$\tau_z = (\frac{1}{2})c\hat{z}$].
[b] τ_x is the translation of half of the a_1 lattice parameter along the $\hat{x}$ direction [$\tau_x = (\frac{1}{2})a_1\hat{x}$].

TABLE XIX. Normal vibrational mode irreducible representations (Γ^{vib}) for the $A17$ phosphorus phase. Irreducible representations for the Raman active, infrared active, acoustic, and silent modes are identified.

D_{2h}^{18} ($Aema$, #64)	
Γ^{vib}	$2\Gamma_1^+ \oplus \Gamma_2^+ \oplus 2\Gamma_3^+ \oplus \Gamma_4^+ \oplus \Gamma_1^- \oplus 2\Gamma_2^- \oplus \Gamma_3^- \oplus 2\Gamma_4^-$
Raman	$2\Gamma_1^+ \oplus \Gamma_2^+ \oplus 2\Gamma_3^+ \oplus \Gamma_4^+$
Infrared	$\Gamma_2^- \oplus \Gamma_3^-$
Acoustic	$\Gamma_2^- \oplus \Gamma_3^- \oplus \Gamma_4^-$
Silent	Γ_1^-

TABLE XX. Normal vibrational mode irreducible representations (Γ^{vib}) for the $A7$ phosphorus phase. Irreducible representations for the Raman active, infrared active, acoustic, and silent modes are identified.

D_{3d}^{5} ($R\bar{3}m$, #166)	
Γ^{vib}	$3(\Gamma_1^+ \oplus \Gamma_3^+ \oplus \Gamma_2^- \oplus \Gamma_3^-)$
Raman	$3(\Gamma_1^+ \oplus \Gamma_3^+)$
Infrared	$2(\Gamma_2^- \oplus \Gamma_3^-)$
Acoustic	$\Gamma_2^- \oplus \Gamma_3^-$
Silent	–

[1] P. W. Bridgman, J. Am. Chem. Soc. **36**, 1344 (1914).
[2] D. Warschauer, J. Appl. Phys. **34**, 1853 (1963).
[3] U. Häussermann, Chem. Eur. J. **9**, 1471 (2003).
[4] Z. Zhu and D. Tománek, Phys. Rev. Lett. **112**, 176802 (2014).
[5] J. Xie, M. S. Si, D. Z. Yang, Z. Y. Zhang, and D. S. Xue, arXiv:1405.4407.
[6] F. Xia, H. Wang, and Y. Jia, Nat. Commun. **5**, 4458 (2014).
[7] V. Tran, R. Soklaski, Y. Liang, and L. Yang, Phys. Rev. B **89**, 235319 (2014).
[8] A. Castellanos-Gomez, L. Vicarelli, E. Prada, J. O. Island, K. L. Narasimha-Acharya, S. I. Blanter, D. J. Groenendijk, M. Buscema, G. A. Steele, J. V. Alvarez, H. W. Zandbergen, J. J. Palacios, and H. S. J. van der Zant, 2D Mater. **1**, 025001 (2014).
[9] A. S. Rodin, A. Carvalho, and A. H. Castro Neto, Phys. Rev. Lett. **112**, 176801 (2014).
[10] S. Zhang, J. Yang, R. Xu, F. Wang, W. Li, M. Ghufran, Y.-W. Zhang, Z. Yu, G. Zhang, Q. Qin *et al.*, ACS nano **8**, 9590 (2014).
[11] P. Li and I. Appelbaum, Phys. Rev. B **90**, 115439 (2014).
[12] R. Fei and L. Yang, Appl. Phys. Lett. **105**, 083120 (2014).
[13] H. Y. Lv, W. J. Lu, D. F. Shao, and Y. P. Sun, Phys. Rev. B **90**, 085433 (2014).
[14] R. Fei, A. Faghaninia, R. Soklaski, J.-A. Yan, C. Lo, and L. Yang, Nano Lett. **14**, 6393 (2014).
[15] H. Y. Lv, W. J. Lu, D. F. Shao, and Y. P. Sun, arXiv:1404.5171.
[16] L. Li, Y. Yu, G. J. Ye, Q. Ge, X. Ou, H. Wu, D. Feng, X. H. Chen, and Y. Zhang, Nat. Nanotech. **9**, 372 (2014).
[17] H. Liu, A. T. Neal, Z. Zhu, Z. Luo, X. Xu, D. Tománek, and P. D. Ye, ACS Nano **8**, 4033 (2014).
[18] J. Qiao, X. Kong, Z.-X. Hu, F. Yang, and W. Ji, Nat. Commun. **5**, 4475 (2014).
[19] S. P. Koenig, R. A. Doganov, H. Schmidt, A. Castro Neto, and B. Oezyilmaz, Appl. Phys. Lett. **104**, 103106 (2014).
[20] M. Buscema, D. J. Groenendijk, S. I. Blanter, G. A. Steele, H. S. van der Zant, and A. Castellanos-Gomez, Nano Lett. **14**, 3347 (2014).
[21] M. Engel, M. Steiner, and P. Avouris, Nano Lett. **14**, 6414 (2014).
[22] O. Frank, G. Tsoukleri, J. Parthenios, K. Papagelis, I. Riaz, R. Jalil, K. S. Novoselov, and C. Galiotis, ACS Nano **4**, 3131 (2010).
[23] H. J. Conley, B. Wang, J. I. Ziegler, R. F. Haglund Jr., S. T. Pantelides, and K. I. Bolotin, Nano Lett. **13**, 3626 (2013).
[24] Y. Wang, C. Cong, C. Qiu, and T. Yu, Small **9**, 2857 (2013).
[25] A. Favron, E. Gaufrès, F. Fossard, P. L. Lévesque, A.-L. Phaneuf-L'Heureux, N. Y.-W. Tang, A. Loiseau, R. Leonelli, S. Francoeur, and R. Martel, arXiv:1408.0345v2.
[26] J. C. Jamieson, Science **139**, 1291 (1963).
[27] J. K. Burdett and S. Lee, J. Solid State Chem. **44**, 415 (1982).
[28] S. E. Boulfelfel, G. Seifert, Y. Grin, and S. Leoni, Phys. Rev. B **85**, 014110 (2012).
[29] J. Guan, Z. Zhu, and D. Tománek, Phys. Rev. Lett. **113**, 046804 (2014).
[30] K. Takeda and K. Shiraishi, Phys. Rev. B **50**, 14916 (1994).
[31] P. Vogt, P. De Padova, C. Quaresima, J. Avila, E. Frantzeskakis, M. C. Asensio, A. Resta, B. Ealet, and G. Le Lay, Phys. Rev. Lett. **108**, 155501 (2012).
[32] L. Li, S.-Z. Lu, J. Pan, Z. Qin, Y.-Q. Wang, Y. Wang, G.-Y. Cao, S. Du, and H.-J. Gao, Adv. Mater. **26**, 4820 (2014).
[33] M. E. Dávila, L. Xian, S. Cahangirov, A. Rubio, and G. Le Lay, New J. Phys. **16**, 095002 (2014).

[34] Y. Xu, B. Yan, H.-J. Zhang, J. Wang, G. Xu, P. Tang, W. Duan, and S.-C. Zhang, Phys. Rev. Lett. **111**, 136804 (2013).
[35] C. J. Bradley and A. P. Cracknell, *The Mathematical Theory of Symmetry in Solids: Representation Theory for Point Groups and Space Groups* (Oxford University Press, New York, 1972).
[36] M. Tinkham, *Group Theory and Quantum Mechanics* (Dover Publications, Mineola, New York, 2012).
[37] P. W. M. Jacobs, *Group Theory with Applications in Chemical Physics* (Cambridge University Press, New York, 2005).
[38] M. S. Dresselhaus, G. Dresselhaus, and A. Jorio, *Group Theory: Application to the Physics of Condensed Matter* (Springer-Verlag Berlin, Heidelberg, Germany, 2008).
[39] *International Tables for Crystallography*, edited by T. Hahn, 5th ed. (Springer, Dordrecht, The Netherlands, 2005), Vol. A: Space-Group Symmetry.
[40] *International Tables for Crystallography*, 1st ed., edited by T. Kopský and D. B. Litvin (Kluwer Academic Publishers, Dordrecht, The Netherlands, 2002), Vol. E: Subperiodic groups.
[41] L. M. Malard, M. H. D. Guimarães, D. L. Mafra, M. S. C. Mazzoni, and A. Jorio, Phys. Rev. B **79**, 125426 (2009).
[42] J. Ribeiro-Soares, R. M. Almeida, E. B. Barros, P. T. Araujo, M. S. Dresselhaus, L. G. Cançado, and A. Jorio, Phys. Rev. B **90**, 115438 (2014).
[43] M. Huang, H. Yan, C. Chen, D. Song, T. F. Heinz, and J. Hone, Proc. Natl. Acad. Sci. USA **106**, 7304 (2009).
[44] T. M. G. Mohiuddin, A. Lombardo, R. R. Nair, A. Bonetti, G. Savini, R. Jalil, N. Bonini, D. M. Basko, C. Galiotis, N. Marzari, K. S. Novoselov, A. K. Geim, and A. C. Ferrari, Phys. Rev. B **79**, 205433 (2009).
[45] S. Sugai and I. Shirotani, Solid State Commun. **53**, 753 (1985).
[46] D. Xiao, G. B. Liu, W. Feng, X. Xu, and W. Yao, Phys. Rev. Lett. **108**, 196802 (2012).
[47] Q. H. Wang, K. Kalantar-Zadeh, A. Kis, J. N. Coleman, and M. S. Strano, Nat. Nanotechnol. **7**, 699 (2012).
[48] Y. Li, Y. Rao, K. F. Mak, Y. You, S. Wang, C. R. Dean, and T. F. Heinz, Nano Lett. **13**, 3329 (2013).
[49] L. M. Malard, T. V. Alencar, A. P. M. Barboza, K. F. Mak, and A. M. de Paula, Phys. Rev. B **87**, 201401(R) (2013).
[50] H. Zeng, G.-B. Liu, J. Dai, Y. Yan, B. Zhu, R. He, L. Xie, S. Xu, X. Chen, W. Yao, and X. Cui, Sci. Rep. **3**, 1608 (2013).